Research Square

Preprints are preliminary reports that have not undergone peer review.
They should not be considered conclusive, used to inform clinical practice,
or referenced by the media as validated information.

Reactive Oxygen Pool over Ceria Enables Catalytic Oscillation

Jie Yan
College of Chemistry and Molecular Engineering, Peking University
Maolin Wang
College of Chemistry and Molecular Engineering, Peking University
Junzhong Xie
College of Chemistry and Molecular Engineering, Peking University
Yapeng Zhao
School of Mathematical Sciences, Peking University
Xianghui Shi
Beijing International Center for Mathematical Research, Peking University
Yuxiong Hu
School of Physical Science and Technology, ShanghaiTech University
Shixiang Yu
College of Chemistry and Molecular Engineering, Peking University
Xingwu Liu
College of Chemistry and Molecular Engineering, Peking University
Mingyu Chu
College of Chemistry and Molecular Engineering, Peking University
Jie Zhang
College of Chemistry and Molecular Engineering, Peking University
Chaowu Xue
School of Physical Science and Technology, ShanghaiTech University
Shuheng Tian
College of Chemistry and Molecular Engineering, Peking University
Yaxuan Wang
College of Chemistry and Molecular Engineering, Peking University
Zijun Peng
College of Chemistry and Molecular Engineering, Peking University
Wu Zhou
School of Physical Sciences and CAS Key Laboratory of Vacuum Physics, University of Chinese Academy of Sciences
Hiroyuki Asakura
Department of Applied Chemistry, Graduate School of Science and Engineering, Kindai University

Meng Wang
College of Chemistry and Molecular Engineering, Peking University
Zhiqiang Li
zli@math.pku.edu.cn

School of Mathematical Sciences, Peking University
Zhu-Jun Wang
wangzhj3@shanghaitech.edu.cn

School of Physical Science and Technology, ShanghaiTech University
Ding Ma
dma@pku.edu.cn

College of Chemistry and Molecular Engineering, Peking University

---

Research Article

Keywords:

Posted Date: April 1st, 2026

DOI: https://doi.org/10.21203/rs.3.rs-9275333/v1

License: This work is licensed under a Creative Commons Attribution 4.0 International License.
Read Full License

Additional Declarations: The authors declare no competing interests.

Reactive Oxygen Pool over Ceria Enables Catalytic Oscillation

Jie Yan[1†], Maolin Wang[1†], Junzhong Xie[1†], Yapeng Zhao[3†], Xianghui Shi[4†], Yuxiong Hu[2], Shixiang Yu[1,5], Xingwu Liu[1], Mingyu Chu[1], Jie Zhang[1], Chaowu Xue[2], Shuheng Tian[1], Yaxuan Wang[1], Zijun Peng[1], Wu Zhou[5], Hiroyuki Asakura[6], Meng Wang[1], Zhiqiang Li[3,4*], Zhu-Jun Wang[2*], Ding Ma[1*].

1. Beijing National Laboratory for Molecular Sciences, New Cornerstone Laboratory, College of Chemistry and Molecular Engineering, Peking University, Beijing 100871, China

2. School of Physical Science and Technology, ShanghaiTech University, 201210, Shanghai, China.

3. School of Mathematical Sciences, Peking University, Beijing 100871, China.

4. Beijing International Center for Mathematical Research, Peking University, Beijing 100871, China

5. School of Physical Sciences and CAS Key Laboratory of Vacuum Physics, University of Chinese Academy of Sciences, Beijing 100049, China

6. Department of Applied Chemistry, Graduate School of Science and Engineering, Kindai University, 3-4-1 Kowakae, Higashi-Osaka, Osaka 577-8502, Japan

† These authors contributed equally to this work.

* Corresponding authors. Email: Ding Ma (dma@pku.edu.cn), Zhu-Jun Wang (wangzhj3@shanghaitech.edu.cn), Zhiqiang Li (zli@math.pku.edu.cn).

Abstract:

Heterogeneous catalytic reactions often exhibit kinetic oscillations—spontaneous, non-equilibrium phenomena occurring across various reaction systems. Despite decades of investigations, the mechanisms that initiate and sustain these oscillations remain elusive. Here we report the discovery of unexpected kinetic oscillations over Pt/CeO_2 catalysts during the competitive oxidation of hydrogen and carbon monoxide at approximately 60 °C. Through *operando* characterization and first-principles mathematical analysis, we uncover the underlying mechanism and existence conditions of oscillations, demonstrating that these oscillations are governed by periodic cycles of ceria reduction and oxidation, gated by CO coverage on Pt. This represents the first demonstration that the reactive oxygen pool of the support can actively induce and sustain catalytic oscillations. These findings redefine metal-support synergy and provide a theoretical formalism for understanding complex non-equilibrium phenomena in heterogeneous catalysis.

Main Text:

Oscillatory chemical reactions, most famously epitomized by the Belousov–Zhabotinsky reaction, manifest as periodic fluctuations in reactant concentrations that defy steady-state expectations(*1-7*). In the realm of heterogeneous catalysis, these non-equilibrium dynamics—particularly during the catalytic oxidation of CO(*8-10*), H_2(*11*), and hydrocarbons(*12, 13*)—have provided a rich window into surface phase transitions and reaction kinetics(*14, 15*). Historically, such oscillations have been attributed almost exclusively to the metal phase(*10, 15-21*). Classical models, such as those pioneered by Ertl *et al.* on Pt(110), link kinetic cycles to reversible surface reconstructions or periodic changes in the metal's oxidation state(*16*). While *in-situ* and *operando* techniques—including transmission electron microscopy (TEM) and X-ray diffraction (XRD)—have refined our view of these nanoscale structural transformations(*17*), the prevailing metal-centric paradigm often overlooks a critical component of the catalytic architecture: the oxide support. Reducible oxides, such as CeO_2, are known to govern steady-state reactivity through strong metal–support interactions (SMSIs) and direct participation in redox cycles(*22-30*). However, the role of these supports in driving non-equilibrium, oscillatory behavior remains largely underexplored.

Here, we report a previously unobserved self-sustained oscillatory phenomenon during the competitive oxidation of CO and H_2 over Pt/CeO_2 catalysts at ~60 °C. Unlike traditional oscillations

confined to the metal surface, this behavior emerges from a dynamic interplay between Pt and the reactive oxygen pool (ROP) within the ceria support. Using a suite of *operando* techniques—including X-ray absorption spectroscopy (XAS), diffuse reflectance infrared Fourier transform spectroscopy (DRIFTS), and environmental scanning electron microscopy (ESEM)—we demonstrate that the oscillations of CO and H_2 oxidation are regulated by CO coverage on Pt sites, which is modulated by the ROP. At low ROP levels, the CO oxidation rate is low, leading to an accumulation of CO coverage that suppresses H_2 oxidation and subsequently promotes the recovery of ROP. Conversely, when ROP increases to a higher level, the enhanced CO oxidation lowers the CO coverage, thereby freeing Pt sites for H_2 oxidation and resulting in the depletion of ROP. Furthermore, we employ a rigorous mathematical framework based on limit cycle theory to validate our proposed mechanism and demonstrate its generalizability across various systems, including single-atom catalysts (Pt_1/CeO_2) and other reducible supports ($Pt/\alpha\text{-}Fe_2O_3$). Our findings not only establish a novel oscillatory mechanism enabled by the ROP in the support, but also provide a representative model system for further studies of non-equilibrium catalytic dynamics.

We initiated our study using a 0.2 wt% Pt/CeO_2 catalyst, with Pt particles averaging 1.3 nm in diameter (Fig. S1–S4 and Table S1). Oscillatory behavior during the competitive oxidation of CO and H_2 ($CO+H_2$ oxidation) was first detected in a temperature-programmed (TP) experiment (**Fig. 1a**). As the temperature increased from 50 °C to 80 °C, oscillations in CO_2 and H_2O formation appeared at approximately 63 °C. Interestingly, although the oscillations vanished at higher temperatures, they re-emerged upon cooling to around 66 °C (**Fig. 1b** and Fig. S5), indicating a reversible temperature threshold for oscillatory behavior.

These oscillations occurred only within a specific range of gas hourly space velocity (GHSV) values (**Fig. 1d**). Generally, lower GHSVs resulted in longer oscillation periods and larger amplitudes. Remarkably, the oscillations were sustained for over 20 hours under isothermal conditions at 62 °C (**Fig. 1e**), indicating exceptional stability. Similar oscillatory behavior was observed across Pt/CeO_2 catalysts with different Pt loadings (Fig. S1 and Fig. S6–S11). In contrast, no oscillations were detected for the 0.2 wt% Pt/SiO_2 catalyst with an inert support (**Fig. 1c**, Fig. S12, and Table S1), underscoring the crucial role of the reducible oxide support.

We first compared the oxidation rates of pure CO, pure H_2, and their mixture. Notably, CO

oxidation was consistently enhanced in the presence of H_2 across all temperatures (**Fig. 2a)**, in agreement with prior reports(*31, 32*). At 30 °C, the H_2 oxidation rate reached 28 s^{-1}—dramatically higher than the CO oxidation rates under CO+H_2 oxidation at 50 °C (0.06 s^{-1}) or pure CO oxidation at 50 °C (0.0004 s^{-1}) (**Fig. 2b**). We need to point out that while CO oxidation rates were measured under kinetic region, H_2 oxidation occurred under full O_2 conversion. These results imply that intrinsic activity for H_2 oxidation is at least four to five orders of magnitude greater than that for CO oxidation.

Importantly, neither pure CO nor pure H_2 oxidation exhibited any oscillatory behavior (**Fig. 2a** and Fig. S13), indicating that the interaction between H_2 and CO is essential for inducing the observed oscillations. For CO+H_2 oxidation over Pt/CeO_2, O_2 is primarily activated on the ceria surface(*22, 33*), while CO and H_2 adsorb and react on Pt sites(*22, 26, 34-37*) (Fig. S14–S15). These processes can be represented by the following steps:

$$\mathrm{CO} + * \longrightarrow \mathrm{CO}*, \qquad (R.1)$$

$$\mathrm{H_2} + 2* \longrightarrow 2\mathrm{H}*, \qquad (R.2)$$

$$\mathrm{O_2} + 2\mathrm{O_V} \longrightarrow 2\mathrm{O_S}, \qquad (R.3)$$

$$2\mathrm{H}* + \mathrm{O_S} \longrightarrow \mathrm{H_2O} + \mathrm{O_V} + 2*, \qquad (R.4)$$

$$\mathrm{CO}* + \mathrm{O_S} \longrightarrow \mathrm{CO_2} + \mathrm{O_V} + *. \qquad (R.5)$$

Here, * denotes Pt surface site, O_S is reactive oxygen on CeO_2, and O_V represents oxygen vacancy on CeO_2.

Due to CO's strong binding affinity for Pt, it can block H_2 adsorption/activation at low temperature (below ~60 °C), effectively suppressing H_2 oxidation (**Fig. 2a**). This inhibition is well-documented(*37, 38*) and further supported by our H–D exchange experiment (Fig. S16). Only when the temperature is sufficiently high (for example, above 66 °C in **Fig. 2a**), does CO react/desorb rapidly enough to free Pt sites, allowing H_2 oxidation to happen. However, these steady-state kinetics alone cannot account for the nonlinear reaction behavior observed.

To investigate the mechanism underlying these self-sustaining oscillations, we employed online MS to monitor gas-phase dynamics. To probe H_2 activation in the presence of CO, we introduced a small amount of D_2 (feed gas: 20 mL/min $CO/O_2/H_2/D_2/Ar$ = 1/1/45/5/48) as a tracer of CO surface coverage (θ_{CO}), which had little effect on the oscillations. Assuming that both the dissociation of H_2 (D_2) and the recombination of H or D atoms to form H_2/D_2/HD readily occur on

the Pt sites (Fig. S15–S16)), by monitoring HD formation in the effluent, we could determine whether H_2 was being adsorbed/activated on the catalyst. A high HD signal corresponds to lower θ_{CO}, reflecting more available Pt sites for H_2 activation.

In CO+H_2 oxidation reaction system, H_2 oxidation rate is governed by θ_{CO}, which reflects CO's inhibition on H_2 activation. Given the rapid adsorption–desorption dynamics of hydrogen (Fig. S16), the ratio of θ_{H^*} (H* coverage) to θ_* (free Pt sites coverage) remains constant, and H_2 adsorption/desorption can be considered in quasi-equilibrium state (detailed in **Supplementary Text**). For simplicity, Pt sites occupied by H are treated as equivalent to free sites. In this scenario, the CO coverage (θ_{CO}) modulates both H_2 oxidation (*R*.6) and CO oxidation (*R*.5):

$$H_2 + O_S + 2* \longrightarrow H_2O + O_V + 2*, \quad (R.6)$$

$$CO* + O_S \longrightarrow CO_2 + O_V + *. \quad (R.5)$$

The corresponding reaction rates are given by:

$$r_1 = k_1 P_{H_2} [O_S] \theta_*^2 = k_1 P_{H_2} [O_S] (1 - \theta_{CO})^2, \quad (eq.1)$$

$$r_2 = k_2 \theta_{CO} [O_S], \quad (eq.2)$$

where k_1 and k_2 are the rate constants for H_2 and CO oxidation, respectively; θ_* is the fraction of unoccupied Pt sites; and $[O_S]$ is the concentration of reactive oxygen on CeO_2. Our experimental data (**Fig. 2a**) suggest that H_2 significantly promotes CO oxidation, implying that k_2 is substantially higher under mixed feed than under pure CO oxidation conditions. Moreover, $k_1 \gg k_2$, highlighting the ultra-fast rate of hydrogen oxidation, however, r_1 remains strongly modulated by CO coverage.

Fig. 2d (left) shows four identical oscillations observed during the reaction. For clarity, we analyze one cycle in detail (**Fig. 2d**, right). Based on the rate profiles of H_2 and CO oxidation, we divide the oscillatory process into three stages (i, ii, and iii).

Before **stage i** (end of oscillation 2), the HD concentration is low, reflecting a high θ_{CO} and an almost complete suppression of H_2 oxidation ($r_1 \approx 0$). Under these conditions, the surface oxygen concentration ($[O_S]$) is high and CO oxidation proceeds rapidly (r_2 dominates the surface reaction kinetics).

Stage i—Onset of H_2 activation

As CO oxidation activity increases, CO coverage decreases slightly. This is evidenced by the small drop in CO* band intensity at 2062 cm^{-1} in *operando* DRIFTS–MS spectra (**Fig. 2e**). Although

θ_{CO} remains high, it is no longer equal to 1, meaning that a small fraction of Pt sites becomes available for H_2 adsorption and activation. This is confirmed by the sharp rise in the HD signal (**Fig.2d**) and the emergence of *OH (or H_2O*) features in the 3000–3600 cm^{-1} region, resulting from hydrogen activation on Pt and subsequent spillover onto the CeO_2 surface. While at this point $(1-\theta_{CO})^2$ in *eq.*1 is small, it is not zero. Considering that hydrogen oxidation is at least four to five orders of magnitude faster than CO oxidation ($k_1 \gg k_2$), even a limited number of free Pt sites enables rapid and abundant H_2 consumption (large r_1), leading to substantial H_2O formation (its MS signal appears with a delay due to re-adsorption on the catalyst/reactor-wall) (**Fig. 2d** and Fig. S18). Notably, the presence of *OH (or H_2O*) due to hydrogen activation also promotes CO oxidation, resulting in a further increase in CO consumption and a concomitant increase in CO_2 formation (*39, 40*).

Stage ii—Cessation of surface reactions: depletion of ROP

This stage is characterized by a rapid decline in the CO and H_2 oxidation rates, accompanied by a fast decrease of HD signal, indicating an increase in $\theta_{CO.}$ In the end, all surface reactions on the catalyst come to a halt (CO and H_2 oxidation, and H-D exchange). According to *eq*.1 and *eq*.2, the simultaneous cessation of both oxidation reactions (r_1=r_2=0) can only occur when the reactive surface oxygen concentration ($[O_S]$) approaches zero since both oxidation processes rely on it. Quantitative analysis shows that the total oxygen consumed during stages i–ii (11.7 μmol) far exceeds the oxygen supplied in gas-phase (0.4 μmol), implicating the depletion of CeO_2's ROP (10.9 μmol, Fig. S19 and **Supplementary Text**). This interpretation is corroborated by the increase of Ce^{3+} signal at 2127 cm^{-1} in the DRIFTS spectra (**Fig. 2e**)(*41*). Once the ROP is exhausted, both CO and H_2 oxidation rates are nearly zero (*R*.5 and *R*.6), CO accumulates on Pt (very high θ_{CO}, close to 1), and thus H–D exchange becomes strongly suppressed.

Stage iii—Reoxidation of CeO_2 and regeneration of oscillatory conditions

At the start, θ_{CO} is still high (and HD remains low), and H_2 oxidation is totally blocked. Gas-phase O_2 is nearly depleted, and no oxygenated products are detected, suggesting oxygen replenishment occurs on CeO_2 vacancies formed during stages i–ii. The gradual decrease in Ce^{3+} signal intensity in DRIFTS spectra further confirms that ceria is slowly re-oxidized in this stage (**Fig. 2e**). This reoxidation progressively restores $[O_S]$ and CO oxidation activity, returning the system (as illustrated in **Fig. 2d**) to conditions resembling those of stage i.

These results highlight the central role of CO coverage in governing the oscillatory behavior. To further verify this, we varied the CO concentration in the feed during H_2 oxidation over the 0.2 wt% Pt/CeO_2 catalyst at 60 °C. As shown in **Fig. 2c**, oscillations occurred only within a specific CO concentration range. At low CO concentration (0.25 %), θ_{CO} is too low to suppress H_2 oxidation, leading to complete O_2 consumption in gas phase. At high CO concentration (1.25 %), H_2 oxidation is strongly inhibited. In both cases, oscillations disappear. Moreover, pulsing a small amount of CO into reactor at the end of stage iii increases θ_{CO} and delays the onset of the next oscillation (Fig. S20). Together, these results confirm that θ_{CO} is the key parameter controlling the initiation and timing of oscillations.

If the above conclusion holds, the electronic state of ceria should also oscillate, reflecting the sharp depletion and replenishment of its reactive oxygen pool (ROP). To verify this, *operando* quick X-ray absorption near-edge structure (QXANES) experiments were conducted at the Ce *K-edge,* with the outlet gas simultaneously monitored by online MS (Fig. S21). Because the temporal resolution of QXANES was lower than the oscillatory frequency, individual cycles could not be resolved. Owing to the stability of the oscillations, the states of the catalysts with the same phase (φ) in the oscillations are identical; thus, φ can be used to represent the state of the catalysts in the oscillations. For the convenience of analysis, the end of stage ii was set to zero ($\varphi = 0$), enabling phase-resolved analysis of the ceria redox dynamics, and φ of each QXANES spectrum can be calculated based on the MS signal of CO_2 (**Fig. 3a**, detailed in **Supplementary Text**). In addition, the scan period of QXANES was set to be slightly longer than the period of the oscillations; here, φ of each QXANES spectrum moves forward to ensure that enough states of the catalyst are observed during oscillations (**Fig. 3a** and movie S1).

Operando Ce *K*-edge QXANES revealed pronounced periodic shifts in the absorption edge energy ($\Delta E = E_{edge}$ - 40440 eV), a direct measure of the Ce^{3+}/Ce^{4+} ratio(*42*) (Fig. S22). During oscillations, the ΔE of Ce *K*-edge XANES periodically changed within a range of ~ 1 eV (**Fig. 3b**, **Fig. 3c**, and Fig. S23); this confirmed the periodic variation of the oxidation state of ceria. Correlating ΔE with φ showed an abrupt drop to ~ –1.2 eV as φ approached 2π, corresponding to rapid $Ce^{4+} \rightarrow Ce^{3+}$ reduction, followed by a gradual increase associated with reoxidation of Ce^{3+} to Ce^{4+} (**Fig. 3d**). This periodic variation agrees well with the mechanism inferred from gas-phase analysis (**Fig. 2d and Fig. 2e**), in which ceria is reduced during stages i–ii and slowly re-oxidized

in stage iii. The strong statistical correlation between ΔE and φ across multiple oscillation cycles (Fig. S24–S26) further confirms the intrinsic periodic redox behavior of ceria. Additionally, ΔE decreased to a low value in H_2 atmosphere and rapidly increased to a high value in O_2 atmosphere; this provided compelling evidence that the Ce^{3+} concentration underwent periodic changes during oscillations (**Fig. 3e**).

The redox dynamics revealed by QXANES are fully consistent with *operando* X-ray diffraction (XRD) and *in-situ* environmental scanning electron microscopy (ESEM) results. *Operando* XRD showed periodic changes in the CeO_2 (220) reflection intensity and position (Fig. S27–S28), corresponding to reversible lattice contraction and expansion during reduction and oxidation of ceria. This, again, confirmed the oscillation of oxide lattice parameters which was in good agreement with *Operando* XANES observation. Meanwhile, *in-situ* ESEM directly visualized oscillatory brightness variations of the catalyst surface (**Fig. 4a** and movie S2). Regions with higher Ce^{3+} content appear brighter because of their lower work function relative to Ce^{4+}, confirming that the observed brightness oscillations originate from the periodic Ce^{3+}/Ce^{4+} transitions(*43, 44*).

Moreover, when a small pulse of $^{18}O_2$ (0.17 μmol) was introduced during oscillations, $C^{16}O^{18}O$ continued to be detected over multiple subsequent cycles (**Fig. 4b**). This persistence indicates that the reactive oxygen pool (ROP) in ceria participates actively but is only partially consumed in each oscillation, consistent with picture that reactive oxygen species are stored as a surface-accessible pool on ceria.

In contrast, *operando* Pt L_3-edge XANES revealed that the white-line intensity remained constant at 0.269 ± 0.003 throughout the oscillations **(Fig. 3f** and Fig. S29–S32), lying between the fully oxidized and reduced reference states (**Fig. 3g**). This indicates that the electronic state of Pt remains unchanged. Consistent EXAFS analysis confirmed stable Pt–Pt coordination and particle size (Fig. S8, Fig. S33–S34, and Table S2).

Together, these results firmly establish that the redox oscillations occur within the ceria support—driven by the dynamic depletion and replenishment of its reactive oxygen pool, gated by CO coverage on Pt sites—while Pt remains structurally and electronically stable.

Based on analysis above, we propose the mechanism shown in **Fig. 4c** (movie S1). In stage i, H_2 promotes CO* oxidation via *R*.7, reducing θ_{CO} and exposing Pt sites for H_2 activation. Since H_2 oxidation is several orders of magnitude faster than CO oxidation, it rapidly depletes both gas-phase

O_2 and the ROP of CeO_2 (stage ii), leading to a decrease in $[O_S]$ and suppression of both oxidation reactions. In stage iii, CO reoccupies Pt, inhibiting H_2 oxidation. The CeO_2 support is gradually re-oxidized, replenishing $[O_S]$ until CO is consumed, thereby restoring the condition necessary for the next oxidation cycle.

Although the oscillatory process has been identified, the underlying reason why the system exhibits sustained oscillations rather than reaching a steady state remains unclear. The transition from steady states to oscillatory dynamics is well understood through dissipative dynamical systems theory. Oscillations typically correspond to attractors, such as chaotic Lorenz attractors or stable limit cycles(*45, 46*). Since the observed oscillations are periodic and robust, they align with the mathematical definition of a stable limit cycle, often arising from auto-catalytic steps within reaction networks(*13, 15, 47*).

Under our reaction conditions, CO and H_2 oxidation compete, providing negative feedback that tends to stabilize the system. During stage i (**Fig. 2d**), however, the H_2 oxidation rate rises sharply, indicating the existence of an auto-catalytic pathway. A likely step is H-assisted CO oxidation:

$$CO* + O_S + * \xrightarrow{H_2} CO_{2,g} + O_V + 2*. \qquad (R.7)$$

Here, as free Pt sites (*) in the presence of H_2 can promote CO oxidation and generate additional free Pt sites (*), it forms an auto-catalytic loop.

Since H_2 and free Pt sites (*) may promote CO oxidation through the formation of *OH (or H_2O*) (*39, 40*), we added H_2O to the feed gas to see whether the presence of *OH (or H_2O*) can also induce oscillation. Under this condition, the promotion arises mainly from H_2O rather than free Pt sites (*) and H_2. However, as shown in Fig. S35, the auto-catalytic step (*R*.7) is not active and no oscillation is observed. This confirms the essential role of the auto-catalytic step (*R*.7).

To interrogate the origin of the oscillations, we developed a reduced kinetic model based on reactions *R*.1–*R*.7 with two key variables: the surface oxygen concentration ($[O_S]$) and the coverage of free Pt site (θ_*). Their dynamics are governed by coupled nonlinear ordinary differential equations (ODEs) that capture the essential reaction steps (**Fig. 5a**, detailed in **Supplementary Text**). In this model, k_{H_2}, k_{CO}, and k_{O_2} represent the activation rate constants of H_2, CO, and O_2, respectively (**Fig. 5d**). The parameter l is the rate constant for CO* oxidation, which is primarily controlled by the activity of surface oxygen, and a quantifies the amount of reactive oxygen in the

reactive oxygen pool (ROP). In addition, n_{Pt} is the number (or density) of Pt sites, and c is the flow-in rate of CO in feed gas.

Numerical simulations show that for specific parameter sets, trajectories from different initial conditions converge asymptotically to a cycle (**Fig. 5b**), producing periodic oscillations in CO and H_2 oxidation rates (Fig. S36). This confirms that the reduced kinetic model predicts a stable limit cycle (periodic oscillations).

Although numerical simulation is useful for exploring dynamical behavior, it offers limited insight into why oscillations occur and under what conditions they persist. More broadly, many reports of chemical oscillations remain largely phenomenological, with limited mechanistic analysis. From the mathematical perspective, well-established frameworks such as bifurcation theory—including limit cycle analysis—can provide systematic and rigorous tools for analyzing oscillatory systems, enabling investigation beyond numerical simulation into the fundamental mechanisms that determine oscillatory behavior. Here, we integrate bifurcation theory with our kinetic model to go beyond simulation and identify the intrinsic criteria that govern the emergence of oscillations. This mathematical perspective offers mechanistic clarity in a way analogous to how group theory classifies crystal structures(*48*) and Fourier analysis underpins infrared spectroscopy(*49*).

Specifically, we apply the Andronov–Hopf bifurcation theorem—a cornerstone in bifurcation theory—to investigate the intrinsic properties of the observed oscillations and to elucidate the mechanisms that determine their occurrence and sustenance. To establish this, we proceed in two steps (detailed in **Supplementary Text**). The first step is to assess the stability of the system's steady state, which is determined by the trace of the system's Jacobian matrix (Tr(***J***)): the steady state is stable when Tr(***J***) < 0 and becomes unstable when Tr(***J***) > 0. Here the sign of Tr(***J***) is determined by parameters (such as $k_{\mathrm{H_2}}$ and k_{CO}) in the model. The second step is to identify whether the instability leads to a stable limit cycle (exhibiting sustained oscillations) by verifying three critical conditions. Thereby, the Andronov–Hopf bifurcation theorem not only validates the emergence of sustained oscillations but also helps us deduce the parameter ranges supporting sustained oscillations, revealing the influence of metal and support on oscillations and extending the oscillatory mechanism to other catalysts.

As shown in **Fig. 5d**, the metal component in the metal/oxide interfacial catalyst primarily affects the rate constants for H_2 activation ($k_{\mathrm{H_2}}$) and CO adsorption (k_{CO}). Our Andronov–Hopf

bifurcation analysis (detailed in **Supplementary Text**) shows that oscillations occur only within bounded ranges of k_{H_2} and k_{CO} (colored regions in **Fig. 5c**), where the steady state becomes unstable and a stable limit cycle emerges. Under this analysis, oscillations are not limited to Pt nanoparticles on ceria (as shown in **Fig. 1 and 2**), they persist even when Pt is present as isolated single atoms (Pt_1) on ceria, as the k_{H_2} and k_{CO} fall within the oscillatory window. Indeed, when the Pt species evolve from isolated single atoms to particles, the oscillatory behavior in CO+H_2 oxidation can be clearly resolved (Fig. S38–S40).

Even when the active metal is replaced by Ru (**Fig. 5c** and Fig. S41) or Pd (Fig. S42), oscillations persist, demonstrating the generality of this phenomenon among metals that have strong interaction with CO (which leads to CO-gated hydrogen adsorption/activation as discussed previously). In contrast, for metals with weak CO binding (low k_{CO}), CO cannot effectively inhibit H_2 activation, and oscillations disappear, as observed for Au/CeO_2 catalyst (Fig. S43). Conversely, for Cu/CeO_2 catalyst, k_{H_2} is too low that the H_2 oxidation rate is insufficient to deplete gas-phase O_2, eliminating the competition between CO and H_2 oxidation (Fig. S44, 2000–2500 s). As a result, Cu/CeO_2 lies outside the oscillatory region in **Figure 5c**. Together, these findings highlight that the dynamic interplay between CO and H_2 oxidation, governed by the metal–support synergy, is essential for sustaining oscillations.

The oxide support also strongly influences oscillatory behavior by controlling the amount (a) and activity (l) of surface oxygen species. Similar to k_{H_2} and k_{CO}, oscillations occur only within bounded ranges of a and l (colored in **Fig. 5e**). When the support is changed from CeO_2 (BASF) to other active oxides—such as CeO_2 nanopolyhedra, CeO_2 nanorods, or α-Fe_2O_3—oscillations are maintained (Fig. S45–S46). However, replacing the support with relatively inert oxides such as TiO_2 and SiO_2 suppresses oscillations completely (**Fig. 1c** and Fig. S47–S48). These observations confirm the indispensable role of ROP in enabling self-sustained catalytic oscillations.

Overall, our mathematical analysis provides a general framework for identifying, in a multidimensional parameter space, which metal/oxide interfacial catalysts are expected to oscillate. By mapping interface-dependent kinetic parameters onto an "oscillatory window," the model enables prediction of whether a given interfacial catalyst will sustain a stable limit-cycle oscillation.

In summary, this work reveals a previously unobserved support-enabled oscillatory phenomenon and elucidates the mechanism governing these dynamics through operando

characterization and isotopic labeling. By integrating systematic mathematical analysis with experimental observations, we establish a rigorous framework that extends beyond numerical simulation and provides fundamental insight into the origin of catalytic oscillations. Our findings advance understanding of oscillatory kinetics and, more broadly, clarify how metal–support interplay and support oxygen storage/release govern interfacial catalysis under reaction conditions.

References

1. R. A. Spangler, F. M. Snell, Sustained oscillations in a catalytic chemical system. *Nature* **191**, 457-458 (1961).
2. E. KÖRÖS, Monomolecular treatment of chemical oscillation. *Nature* **251**, 703-704 (1974).
3. B. P. Belousov, Периодически действующая реакция и ее механизм. *Сборник рефератов по радиационной медицине* **147**, 145-147 (1959).
4. A. M. Zhabotinsky, Периодический процесс окисления малоновой кислоты растворе. *Биофизика* **9**, 306-311 (1964).
5. V. Petrov, V. Gáspár, J. Masere, K. Showalter, Controlling chaos in the Belousov—Zhabotinsky reaction. *Nature* **361**, 240-243 (1993).
6. Y. Suchorski *et al.*, Resolving multifrequential oscillations and nanoscale interfacet communication in single-particle catalysis. *Science* **372**, 1314-1318 (2021).
7. R. Zhang, Y. Wang, P. Gaspard, N. Kruse, The oscillating Fischer-Tropsch reaction. *Science* **382**, 99-103 (2023).
8. H. Beusch, P. Fieguth, E. Wicke, Thermisch und kinetisch verursachte Instabilitäten im Reaktionsverhalten einzelner Katalysatorkörner. *Chem. Ing. Tech.* **44**, 445-451 (1972).
9. G. Ertl, Oscillatory kinetics and spatio-temporal self-organization in reactions at solid surfaces. *Science* **254**, 1750-1755 (1991).
10. A. M. Gänzler *et al.*, Operando spatially and time-resolved X-ray absorption spectroscopy and infrared thermography during oscillatory CO oxidation. *J. Catal.* **328**, 216-224 (2015).
11. Z. Kurtanjek, M. Sheintuch, D. Luss, Surface state and kinetic oscillations in the oxidation of hydrogen on nickel. *J. Catal.* **66**, 11-27 (1980).
12. A. Amariglio, O. Benali, H. Amariglio, Oscillating oxidation of propene on copper oxides. *J. Catal.* **118**, 164-174 (1989).

13. C. G. Vayenas, B. Lee, J. Michaels, Kinetics, limit cycles, and mechanism of the ethylene oxidation on platinum. *J. Catal.* **66**, 36-48 (1980).
14. F. Schüth, B. E. Henry, L. D. Schmidt, Oscillatory reactions in heterogeneous catalysis. *Adv. Catal.* **39**, 51-127 (1993).
15. R. Imbihl, G. Ertl, Oscillatory kinetics in heterogeneous catalysis. *Chem. Rev.* **95**, 697-733 (1995).
16. T. Gritsch, D. Coulman, R. J. Behm, G. Ertl, Mechanism of the CO-induced 1× 2→ 1× 1 structural transformation of Pt (110). *Phys. Rev. Lett.* **63**, 1086 (1989).
17. S. B. A. Vendelbo *et al.*, Visualization of oscillatory behaviour of Pt nanoparticles catalysing CO oxidation. *Nat. Mater.* **13**, 884-890 (2014).
18. B. L. M. Hendriksen *et al.*, The role of steps in surface catalysis and reaction oscillations. *Nat. Chem.* **2**, 730-734 (2010).
19. M. Kim *et al.*, Controlling chemical turbulence by global delayed feedback: pattern formation in catalytic CO oxidation on Pt (110). *Science* **292**, 1357-1360 (2001).
20. L. Sandoval-Diaz *et al.*, Metastable nickel-oxygen species modulate rate oscillations during dry reforming of methane. *Nat. Catal.* **7**, 161-171 (2024).
21. S. Yue *et al.*, Redox dynamics and surface structures of an active palladium catalyst during methane oxidation. *Nat. Commun.* **15**, 4678 (2024).
22. L. Nie *et al.*, Activation of surface lattice oxygen in single-atom Pt/CeO_2 for low-temperature CO oxidation. *Science* **358**, 1419-1423 (2017).
23. J. A. Farmer, C. T. Campbell, Ceria maintains smaller metal catalyst particles by strong metal-support bonding. *Science* **329**, 933-936 (2010).
24. S. Hu, W. X. Li, Sabatier principle of metal-support interaction for design of ultrastable metal nanocatalysts. *Science* **374**, 1360-1365 (2021).
25. X. Li *et al.*, Functional CeO_2 nanoglues for robust atomically dispersed catalysts. *Nature* **611**, 284-288 (2022).
26. J. Jones *et al.*, Thermally stable single-atom platinum-on-ceria catalysts via atom trapping. *Science* **353**, 150-154 (2016).
27. M. Cargnello *et al.*, Exceptional activity for methane combustion over modular Pd@CeO_2 subunits on functionalized Al_2O_3. *Science* **337**, 713-717 (2012).
28. Z. Liu *et al.*, Water-promoted interfacial pathways in methane oxidation to methanol on a CeO_2-Cu_2O catalyst. *Science* **368**, 513-517 (2020).
29. J. A. Rodriguez *et al.*, Activity of CeO_x and TiO_x nanoparticles grown on Au(111) in the water-gas shift reaction. *Science* **318**, 1757-1760 (2007).
30. M. Cargnello *et al.*, Control of metal nanocrystal dize teveals metal-dupport interface role for ceria catalysts. *Science* **341**, 771-773 (2013).
31. M. Shou, K. Tanaka, Isotope effect of H_2/D_2 and H_2O/D_2O for the PROX reaction of CO on the FeO_x/Pt/TiO_2 catalyst. *Catal. Lett.* **111**, 115-118 (2006).
32. M. Daté, M. Haruta, Moisture Effect on CO Oxidation over Au/TiO_2 Catalyst. *J. Catal.* **201**, 221-224 (2001).
33. C. Yang *et al.*, O_2 activation on Ceria catalysts-the importance of substrate crystallographic orientation. *Angew. Chem. Int. Ed.* **56**, 16399-16404 (2017).
34. X. I. Pereira-Hernandez *et al.*, Tuning Pt-CeO_2 interactions by high-temperature vapor-phase synthesis for improved reducibility of lattice oxygen. *Nat. Commun.* **10**, 1358 (2019).

35. K. Ding *et al.*, Identification of active sites in CO oxidation and water-gas shift over supported Pt catalysts. *Science* **350**, 189-192 (2015).
36. J. Lee *et al.*, How Pt influences H_2 reactions on high surface-area Pt/CeO_2 powder catalyst surfaces. *JACS Au* **3**, 2299-2313 (2023).
37. M. Montano, K. Bratlie, M. Salmeron, G. A. Somorjai, Hydrogen and deuterium exchange on Pt(111) and its poisoning by carbon monoxide studied by surface sensitive high-pressure techniques. *J. Am. Chem. Soc.* **128**, 13229-13234 (2006).
38. J. Z. Zhang, K. Hongsirikarn, J. G. Goodwin, The effect of low concentrations of CO on H_2 adsorption and activation on Pt/C: Part 2—In the presence of H_2O vapor. *J. Power Sources* **196**, 6186-6195 (2011).
39. R. A. Ojifinni *et al.*, Water-enhanced low-temperature CO oxidation and isotope effects on atomic oxygen-covered Au(111). *J. Am. Chem. Soc.* **130**, 6801-6812 (2008).
40. J. Saavedra, H. A. Doan, C. J. Pursell, L. C. Grabow, B. D. Chandler, The critical role of water at the gold-titania interface in catalytic CO oxidation. *Science* **345**, 1599-1602 (2014).
41. F. Bozon-Verduraz, A. Bensalem, IR studies of cerium dioxide: influence of impurities and defects. *Angew. Chem. Int. Ed.* **90**, (1994).
42. M. Rothensteiner *et al.*, Ce *K*-edge XAS of ceria-based redox materials under realistic conditions for the two-step solar thermochemical dissociation of water and/or CO_2. *Phys. Chem. Chem. Phys.* **17**, 26988-26996 (2015).
43. H. F. Wardenga, A. Klein, Surface potentials of (111), (110) and (100) oriented CeO_{2-x} thin films. *Appl. Surf. Sci.* **377**, 1-8 (2016).
44. J. Cai *et al.*, Two-dimensional crystalline platinum oxide. *Nat. Mater.* **23**, 1654-1663 (2024).
45. E. Campos-Canton, R. Femat, G. Chen, Attractors generated from switching unstable dissipative systems. *Chaos* **22**, 033121 (2012).
46. M. Sheintuch, Nonlinear kinetics in catalytic oxidation reactions: Periodic and aperiodic behavior and structure sensitivity. *J. Catal.* **96**, 326-346 (1985).
47. J. K. Hale, *Asymptotic behavior of dissipative systems*. Mathematical Surveys and Monographs (American Mathematical Society, Providence, RI, 2010).
48. R. C. Powell, *Symmetry, Group Theory, and the Physical Properties of Crystals*. (Springer, New York, 2010).
49. P. R. Griffiths, Fourier transform infrared spectrometry. *Science* **222**, 297-302 (1983).
50. Y. Wang, J. Ren, K. Deng, L. Gui, Y. Tang, Preparation of Tractable Platinum, Rhodium, and Ruthenium Nanoclusters with Small Particle Size in Organic Media. *Chem. Mater.* **12**, 1622-1627 (2000).
51. M. Brin, G. Stuck, *Introduction to Dynamical Systems*. (Cambridge University Press, Cambridge, 2004), pp. 1–27.
52. S. H. Strogatz. *Nonlinear Dynamics and Chaos.* (Westview Press, 2015), pp. 257–262.
53. J. H. Liu. *A First Course in the Qualitative Theory of Differential Equations*. (Pearson Education, 2003), pp.272–316.
54. J. D. Meiss. *Differential Dynamical Systems*. (Society for Industrial and Applied Mathematics, 2007), pp.267–331.
55. Deshpande, S., Patil, S., Kuchibhatla, S. V. N. T. & Seal, S. Size dependency variation in lattice parameter and valency states in nanocrystalline cerium oxide. *Appl. Phys. Lett.* **87**, 133113 (2005).

Acknowledgments

This work received financial support from Beijing Natural Science Foundation Project (JQ25001), the National Key R&D Program of China (2021YFA1501102), and the National Natural Science Foundation of China (12471083, 22232001, 21932002). XAFS experiments were conducted at 1W1B of the Beijing Synchrotron Radiation Facility (BSRF) and Shanghai Synchrotron Radiation Facility. The *operando* XAS experiments were performed at BL14B2 of SPring-8 with the approval of the Japan Synchrotron Radiation Research Institute (JASRI) (Proposal No. 2023A1678). This research was supported by the CAS Project for Young Scientists in Basic Research (YSBR-003). This research benefited from resources and support from the Electron Microscopy Center at the University of Chinese Academy of Sciences. D.M. acknowledges support from the New Cornerstone Science Foundation through the XPLORER PRIZE and New Cornerstone Investigator Program. We would like to thank Prof. Charles T. Campbell and Prof. Xinhe Bao for reading the manuscript and providing insightful comments.

Author contributions

D. M. conceived and supervised the project. J. Y., J. X., X. L., Y. W. and Z. P. performed most of the reactions. M. W., S. T. and H. A. performed the X-ray related characterizations (XAS) and analysis. S.Y., W. Z., Y. X. and Z-J. W. performed the electron microscopy study. Y. Z., X. S. and Z. L. conduct mathematical analysis. J. Y., M. C., J. Z., M. W., J. X., C. X., Z-J. W. and D. M. wrote the paper. All authors contributed to the discussion and revision of the paper.

Competing interest.

The authors declare no competing interests.

Data availability

The main data supporting the findings of this study are available within the paper and Supporting Information. Additional data are available from the corresponding authors upon reasonable request.

Supplementary Materials

Materials and Methods

Supplementary Text

Figs. S1 to S48

Tables S1 to S2

References (*50*–*55*)

Movies S1 to S2

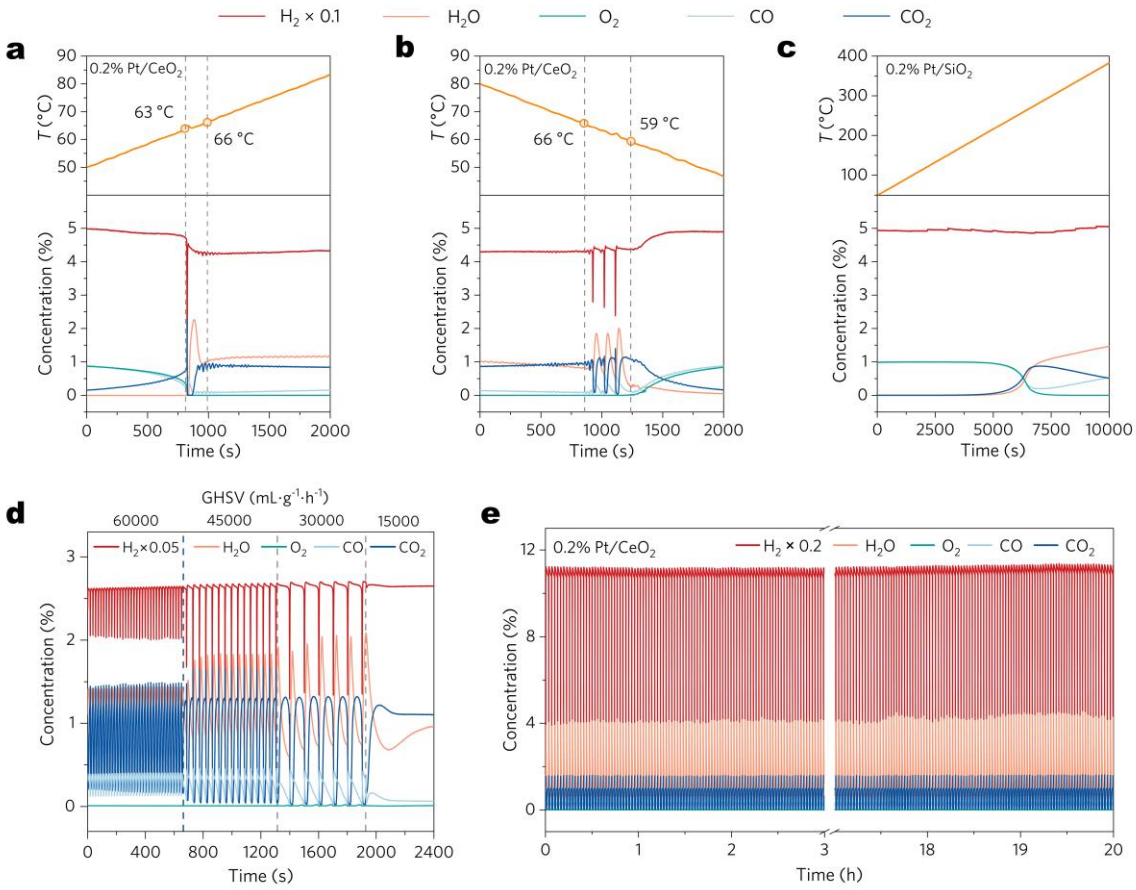

Fig. 1. Observation of CO+H_2 oxidation oscillations over the 0.2 wt% Pt/CeO_2 catalyst. (**a**) Temperature-programmed (TP) CO+H_2 oxidation experiment over 0.2 wt% Pt/CeO_2 (ramping rate: 1 °C/min; feed gas: 20 mL/min CO/O_2/H_2/Ar = 1/1/50/48). (**b**) Oscillation behavior observed in the cooling process after the TP experiment in (**a**) over the 0.2 wt% Pt/CeO_2 catalyst (cooling rate: 1 °C/min; feed gas: 20 mL/min CO/O_2/H_2/Ar = 1/1/50/48). (**c**) TP CO+H_2 oxidation experiment over a 0.2 wt% Pt/SiO_2 catalyst (ramping rate: 2 °C/min; feed gas: 20 mL/min CO/O_2/H_2/Ar = 1/1/50/48). (**d**) Variation in oscillatory behavior with GHSV (gas hourly space velocity) catalyzed by 0.2 wt% Pt/CeO_2 at 58 °C (feed gas: x mL/min CO/O_2/H_2/Ar = 1/1/50/48). (**e**) Stability evaluation for CO+H_2 oxidation oscillations catalyzed by a 0.2 wt% Pt/CeO_2 catalyst (62 °C; feed gas: 20 mL/min CO/O_2/H_2/Ar = 1/1/50/48).

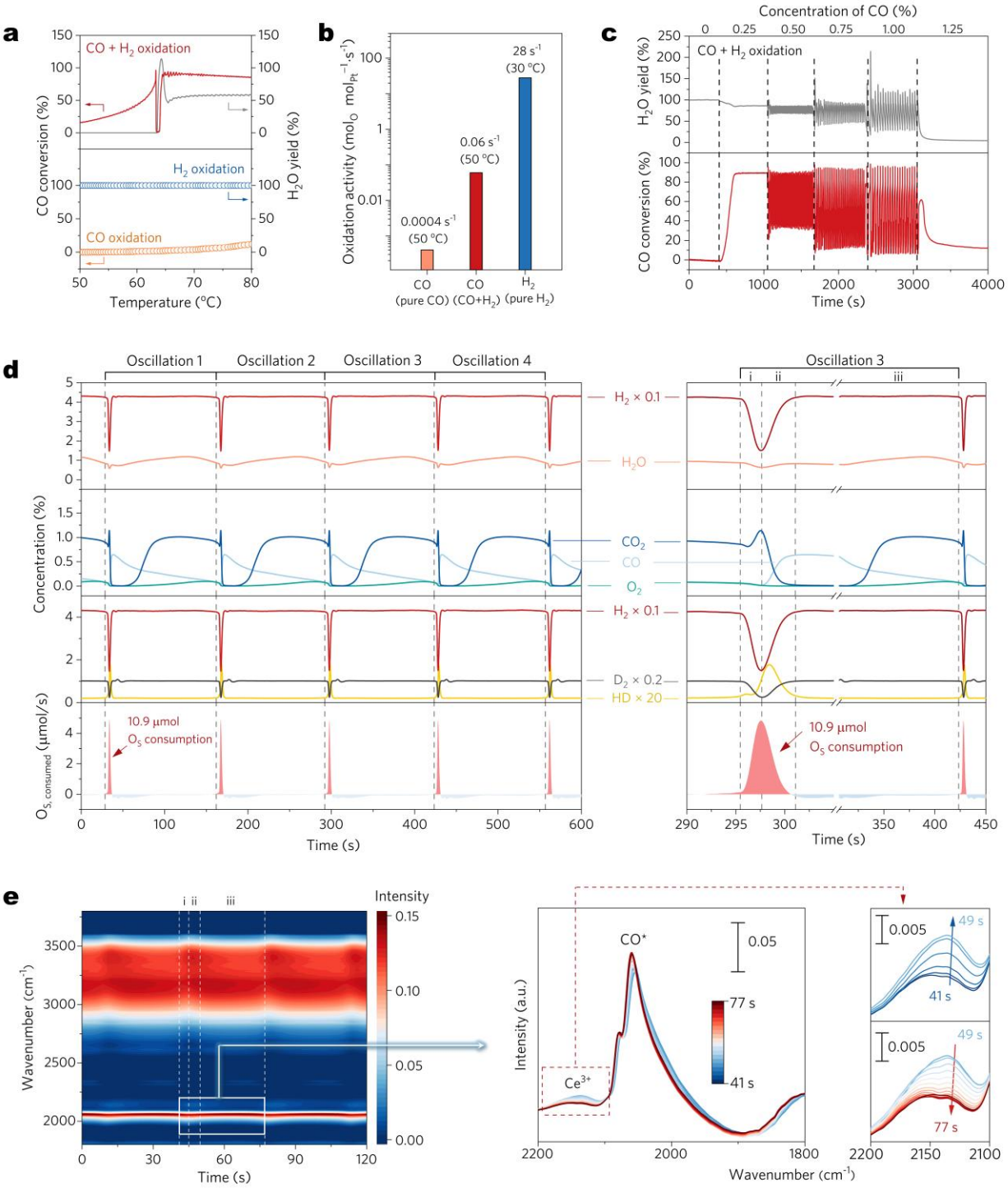

Fig. 2. Mechanistic study of the CO+H_2 oxidation oscillations. (**a**) Comparison of the performance of the CO+H_2 oxidation, CO oxidation, and H_2 oxidation reactions catalyzed by the 0.2 wt% Pt/CeO_2 catalyst (feed gas for CO+H_2 oxidation: 20 mL/min CO/O_2/H_2/Ar = 1/1/50/48; feed gas for CO oxidation: 20 mL/min CO/O_2/Ar = 1/1/98; and feed gas for H_2 oxidation: 100 mL/min O_2/H_2/Ar = 1/50/49). (**b**) Comparison of the reaction rates for pure CO oxidation, CO+H_2 oxidation, and H_2 oxidation reactions. The reaction rates of pure CO oxidation and CO+H_2 were

measured in the kinetic region, whereas for H_2 oxidation the measurement was conducted with full O_2 conversion. Thus, the real intrinsic activity for H_2 oxidation could be much greater. (**c**) Variation in the CO+H_2 oxidation oscillations with increasing CO concentration over 0.2 wt% Pt/CeO_2 (Reaction conditions: 60 °C; feed gas: 40 mL/min O_2/H_2/Ar = 1/50/49, and then 0/0.1/0.2/0.3/0.4/0.5 mL/min CO was added to the feed). (**d**) Gas-phase species analysis during CO+H_2 oxidation oscillations with D_2 co-feed in feed gas. (Reaction conditions: 40 mg 0.2 wt% Pt/CeO_2, 56 °C, and 20 mL/min CO/O_2/H_2/D_2/Ar = 1/1/45/5/48). On the left, four sequenced oscillations are illustrated. Oscillation 3 is enlarged to show the details of the oscillation on the right. The net consumption rate of O_S ($O_{S,\ consumed}$) is calculated through the consumption rate of H_2 (H_2 oxidation rate, including D_2 and HD), the formation rate of CO_2 (CO oxidation rate), and the consumption rate of O_2. (**e**) Evolution of surface species and Ce^{3+} content during oscillations detected by time-resolved *operando* DRIFTS–MS device. Right picture shows the evolution of DRIFTS signal in the region of 1800 ~ 2200 cm^{-1} during one oscillation (41 ~ 77 s). MS signals are shown in Fig. S17**.**

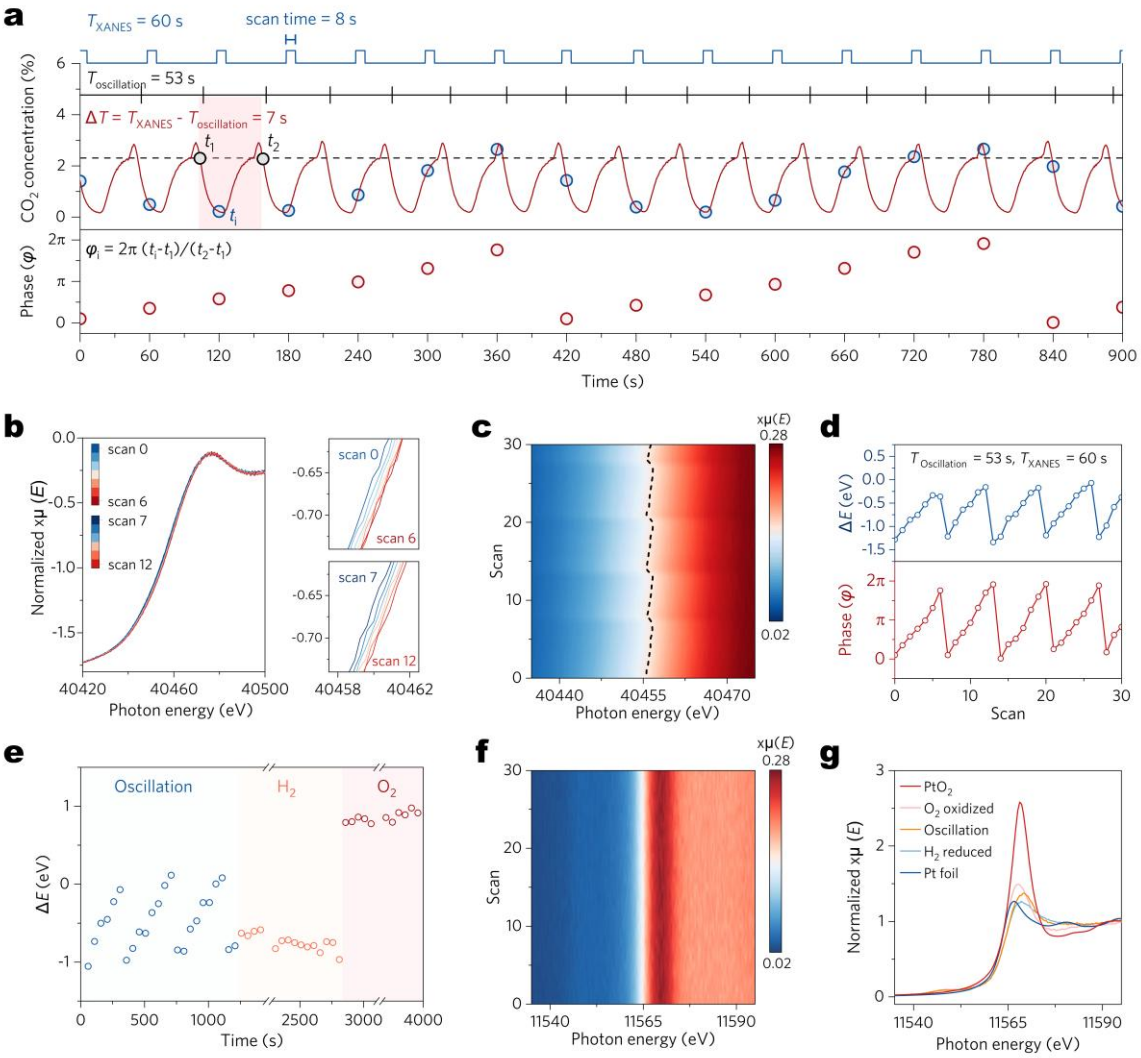

Fig. 3. Evolution of the electronic structure of Ce and Pt species in the CO+H_2 oxidation oscillations. (**a**) Schematic diagram of the method used for the QXANES experiments. The red line represents concentration of CO_2 detected by MS. The blue dots represent the times of QXANES data collection. The dashed line is used to determine the zero point of the phase (φ = 0) for each period of oscillation, and the highlighted region is one complete period from φ = 0 to φ = 2π. The red dots represent the phase of the XANES data collection time. The detailed method is described in Methods. (**b**) Ce *K*-edge QXANES in two representative oscillation periods. (**c**) Ce *K*-edge QXANES over 30 scans with $T_{oscillation}$ = 53 s and T_{XANES} = 60 s. The dashed line represents the periodic change in edge energy (the inflection point of the absorption edge). (**d**) Shift in Ce *K*-edge energy ($\Delta E = E_{edge}$ - 40440 eV) during oscillations and the corresponding phases of oscillations over 30 scans, with $T_{oscillation}$ = 53 s and T_{XANES} = 60 s. (**e**) Shift in the edge energy of the Ce *K*-edge in oscillations, H_2, and O_2 atmospheres. (**f**) Pt L_3-edge QXANES over 30 scans with $T_{oscillation}$ = 36 s

and T_{XANES} = 55 s. The white line intensity remains constant across the different phases over 30 scans (Fig. S29). (**g**) Pt L_3-edge XANES in oscillations, O_2, and H_2 atmospheres, with PtO_2 and Pt foil as reference.

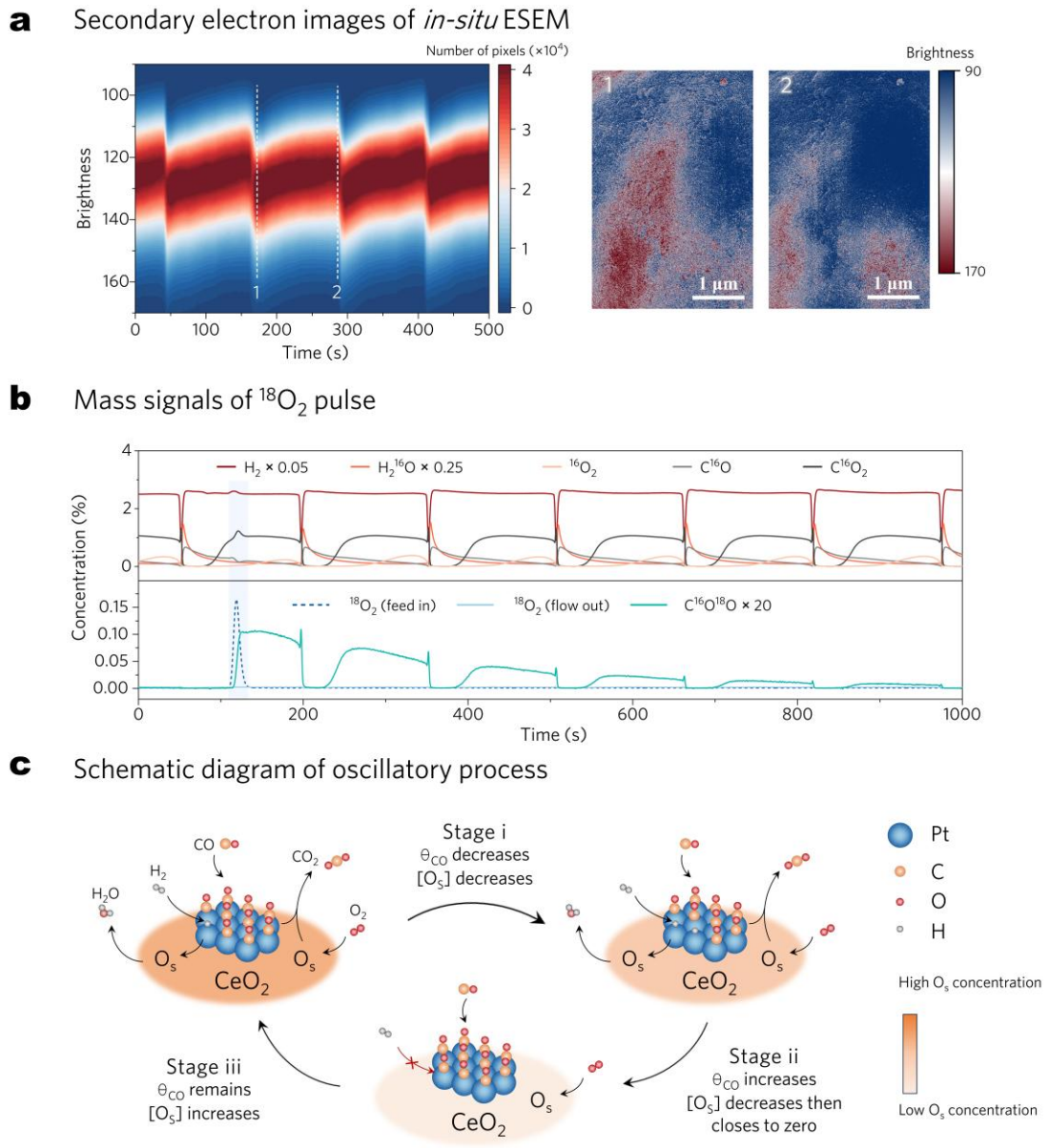

Fig. 4 Participation of the ROP in oscillations. (**a**) Evolution of secondary electron (SE) image brightness during oscillations (see movie S2), with pixel intensity distribution histograms quantifying brightness fluctuations. Right pictures show the different brightness of two SE images during one oscillation. (**b**) Variation of gas-phase reactants/products during oscillations after a $^{18}O_2$ pulse. Temperature: 56 °C. Reaction gas: 15 mL/min CO/$^{16}O_2$/H_2/Ar=1/1/50/48. Pulse gas: 15 mL/min $^{18}O_2$/He/Ar=1/1/98. $^{18}O_2$ (feed in) is obtained through the signal of He and $^{18}O_2$ (flow out) represents the concentration of $^{18}O_2$ in vent gas detected by online MS. (**c**) Schematic diagram of the CO+H_2 oxidation oscillatory process.

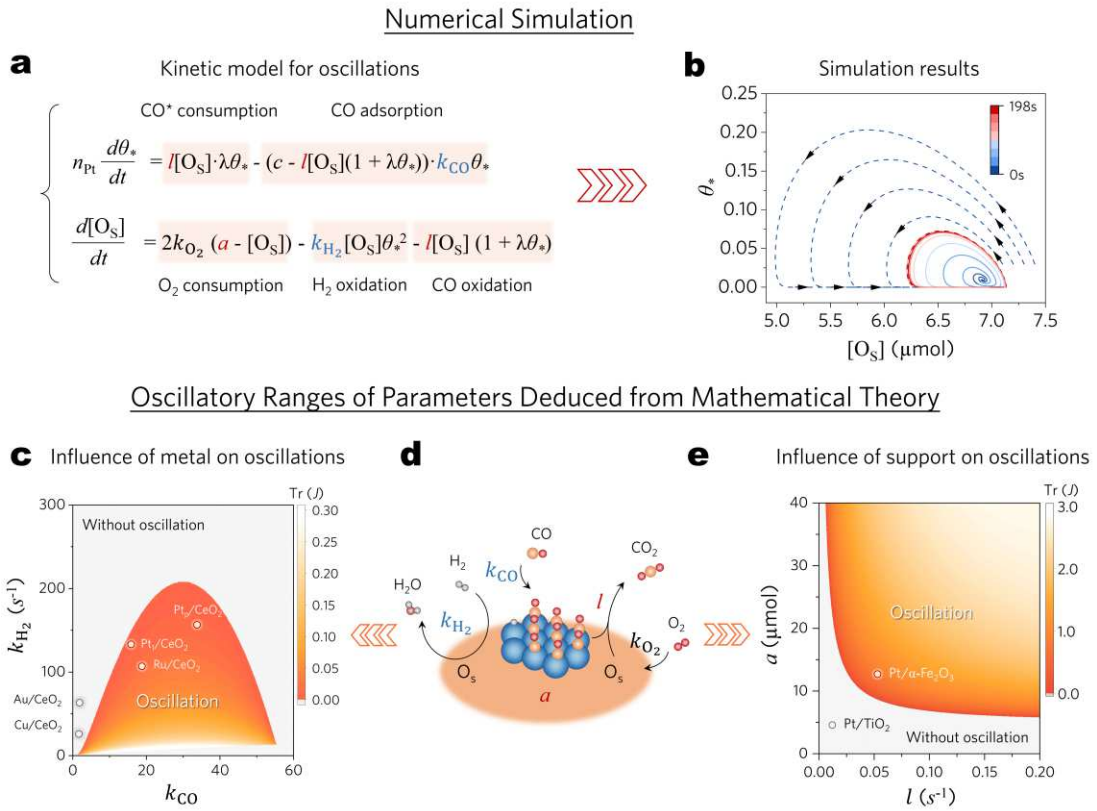

Fig. 5 Mathematical analysis of the oscillatory mechanism. (**a**) Reduced kinetic model of CO+H_2 oxidations' oscillations based on the variation of θ_* and $[O_S]$. In this model, k_{H_2} denotes H_2 oxidation rate constant, k_{CO} denotes CO adsorption rate constant, l denotes CO oxidation rate constant, k_{O_2} denotes O_2 consumption rate constant, a denotes the maximum of $[O_S]$ content, c denotes the flow-in rate of CO in gas phase, and λ denotes promotion effect of θ_* on CO oxidation. (**b**) Simulation results of kinetic model in (a) (detailed in Supplementary Text). (**c**) Influence of metal (k_{H_2} and k_{CO}) on oscillations. Oscillations would only happen in the colored region (Tr(***J***)> 0). The oscillatory performance of the catalysts labelled in the figure are shown in Fig. S38–S44. (**d**) Schematic of the CO+H_2 oxidation. (**e**) Influence of support (a and l) on oscillations. Oscillations would only happen in the colored region (Tr(***J***)> 0). The oscillatory performance of catalysts labelled in the figure are shown in Fig. S46–S48.

Supplementary Files

This is a list of supplementary files associated with this preprint. Click to download.

- SupplementalMaterial.docx
- movieS1.mp4
- movieS22.mp4